Low-cost Test System for 1U CubeSat Attitude Control with Reaction Wheels

Pablo R. Yanyachi
Astronomic and Aerospace Institute
Pedro Paulet - IAAPP
Universidad Nacional de San Agustín
Arequipa, Perú
raulpab@unsa.edu.pe

Hammerly Mamani-Valencia
Astronomic and Aerospace Institute
Pedro Paulet - IAAPP
Universidad Nacional de San Agustín
Arequipa, Perú
hmamaniva@unsa.edu.pe

Brayan Espinoza-García
Astronomic and Aerospace Institute
Pedro Paulet - IAAPP
Universidad Nacional de San Agustín
Arequipa, Perú
bespinozag@unsa.edu.pe

***Abstract*—CubeSat development is becoming one of the most important research topics due to the growing interest of American countries in developing their aerospace technology. The main aim of this work is to simulate a 1U CubeSat Dynamics and develop a test system to allow students to probe their attitude control algorithms. The test system has four parts: a ball-type Dyson sphere air bearing, a Prototype of a CubeSat that includes reaction wheels as actuators, an Onboard computer based on an ARM Cortex M4 TM4C123G, and a PC Software interface. In its preliminary stages, the system allows testing attitude control algorithms for small Euler Angles and monitors reaction wheel parameters such as rates and currents. For the 1U CubeSat simulation, a linear mathematical model, a PID attitude controller, and a PID torque controller are proposed guidelines for attitude control algorithm designs.**

***Keywords*—Attitude control, CubeSat, Attitude Test System, Dyson Sphere, Reaction Wheels.**

I. Introduction

In recent years, aerospace engineering and satellite development have gained importance and popularity due to their applications in telecommunications, geolocation, and remote sensing. Missions such as the James Webb Telescope, the Robert Perseverance, and the advances presented by SpaceX and the Starlink project only increase the interest of the student community in aerospace technology and its applications. As a consequence of this "new space golden age", in 2020 and 2021 alone, 2,907 satellites have begun to orbit our planet. According to the registry of the United Nations Office for Outer Space Affairs (UNOOSA), this amount exceeds by more than 33% all missions currently in orbit. In its early years, satellite aerospace technology had high costs to design, manufacture, and launch into orbit due to its weight and size. This panorama changed with the development of the CubeSat standard, developed in 1999. Since then, small satellites have become popular due to their low weight and size, reducing the costs of development and launching into orbit.

When talking about earth observation satellite systems, one of the most important aspects is their attitude or orientation, which is treated by the attitude determination and control system (ADCS). The attitude is commonly affected by several environmental disturbances capable of generating external torques, which must be corrected by a controller implemented by the ADCS and comply with the Payload requirements such as pointing earth. Various attitude control test systems have been developed over time to design the ADCS system.

According to the Assembly, Integration and Tests (AIT) activities, all satellites undergo a testing process before being launched. CubeSats also require the same test as larger spacecraft, and NASA provides guidelines to perform tests which are: functional test, mechanical test, and vacuum-thermal test [1].

Between functional tests, attitude determination and control subsystem tests are carried out. The development and implementation of a test system for the attitude of Satellites are extensively studied in [2], [3]. Each one of them differs according to the physical parameter to be tested.

For developing an attitude determination and control software for a CubeSat, it is necessary to emulate the condition of zero gravity, for which air bearings are used. The operating principle of an air bearing consists of the constant pressure of tiny holes that collide on a surface, producing a film of air of 5 to 10 μm between both surfaces [4]. The suspended body, due to air pressure, may have friction-free movement. Also, air bearings can be flat or spherical.

Spherical air-bearing consists of a hemispherical plate with holes through pressurized air flows. Air collides with a spherical surface object that makes it float, creating an environment of microgravity. The shape of the floating spherical body will define the degrees of freedom. According to its shape, there are four types: Tabletop, Umbrella, Dumbbell, and Dyson sphere [5]–[7]. Between them, the Dyson sphere type has complete freedom for roll, pitch, and yaw angles and, due to its shape, does not change the CubeSat center of mass.

This article will focus on a test system for attitude control of one Unit CubeSat with three reaction wheels as actuators. The proposed system allows us to test the control algorithms and monitor consumption currents and rates of each reaction wheel. Also, we will be able to see the CubeSat Euler angles. This article shows the implementation of an ADCS test system based on the spherical air bearing method with a Dyson sphere. Here, attitude determination is implemented with the data collected from the sensors. A mathematical model for the ideal balanced CubeSat prototype has been developed, and simu-

978-1-6654-8014-7/22/$31.00

lations of the attitude control algorithms are performed and proposed. This article is divided into the following sections to reach this aim: Section II presents a linear and non-linear mathematical model for an ideally balanced CubeSat. Section II-D explains the transfer function identification process to model our own designed reaction wheels and how to measure the current torque indirectly. Section II-E shows the mathematical model simulations and compares the linear and non-linear models to validate linearization. In section III we talk about the design and implementation of the entire test system, including CubeSat hardware and software, monitoring and control software interface, and the system control algorithm. Finally, the conclusions and recommendations for further research are shown in section V.

II. Mathematical Model

A. Reference frames

Fig. 1a shows the two reference frames necessary for attitude determination. The fixed or orbit frame is denoted by (x, y, z), and the body frame attached to the CubeSat body or body frame is denoted by (x_c, y_c, z_c).

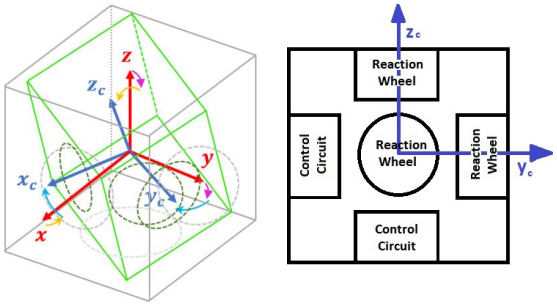

(a) Reference frames (b) CubeSat x_c axis view

Fig. 1. (a) Orbit and body frame where the origin coincides with the center of mass and geometric. (b) CubeSat x_c axis view with balanced payloads; the x_c axis is perpendicular to the paper.

B. Non-linear model

The CubeSat model is given by a dynamic and a kinematic equation. In [8]–[10] a CubeSat with three reaction wheels were modeled by (1), (3), (4).

$$[\dot{\phi}, \dot{\theta}, \dot{\psi}]^T = B(\theta, \phi)\omega \tag{1}$$

Equation (1) represents the kinematic equation where ω is the angular rate vector of the CubeSat in the body frame and ϕ, θ, ψ are roll, pitch, and yaw angles, respectively. $B(\theta, \phi)$ matrix is defined by the Euler Sequence; In the 1-2-3 sequence is defined by (2)

$$B(\theta,\phi) = \begin{bmatrix} 1 & sin(\phi)tan(\theta) & cos(\phi)tan(\theta) \\ 0 & cos(\phi) & -sin(\phi) \\ 0 & \frac{sin(\phi)}{cos(\theta)} & \frac{cos(\phi)}{cos(\theta)} \end{bmatrix} \tag{2}$$

Dynamics equations are described by (3) and (4).

$$\dot{\omega} = J_B^{-1}\left[L - L_{rw} - \omega \times (J_B\omega + J_{rw}\left[\omega + \Omega\right])\right] \tag{3}$$

$$\dot{\Omega} = J_{rw}^{-1}L_{rw} - \dot{\omega} \tag{4}$$

Nomenclature is the same as used in [9]. Where:

- ω: Angular velocity of the satellite relative to the orbit frame.
- J_B: Body inertia tensor with respect to the rotation center.
- $J_{r\omega}$: Total reaction wheel's inertia tensor with respect to the rotation center.
- L: External torque applied to the center of mass expressed in the body frame.
- $L_{r\omega}$: Reaction wheels torque applied to the center of mass expressed in the body frame.
- Ω: Reaction wheels angular rate applied to the center of mass expressed in the body frame.

C. Linear model

Linear equations of motion were founded applying the Euler-Lagrange method [11]–[13], and the linear model was found taking the considerations:

- There is slight friction on the motor bearings.
- Reaction wheels have the same weight and inertia.
- Reaction wheels are balanced with payloads.
- Small Euler angles approximation is used with the CubeSat angular rates (5) [10], [14].

$$\omega = [\dot{\phi}, \dot{\theta}, \dot{\psi}]^T \tag{5}$$

- To be coherent with (3) and (4), we describe the reaction wheels torque (L_{rw}), reaction wheels angular rate (Ω), CubeSat Inertia tensor (J_B), and Reaction Wheels inertia tensor (J_{rw}) as:

$$L_{rw} = [\tau_{wA}, \tau_{wB}, \tau_{wC}]^T,\ \Omega = [\dot{\alpha_A}, \dot{\alpha_B}, \dot{\alpha_C}]^T,$$
$$J_B = Diag([I_b, I_b, I_b]),\ J_{rw} = Diag([I_w, I_w, I_w]),$$

Where the '$Diag()$' operator represents a diagonal matrix.

1) Equations of motion in the x_c axis (Roll): kinetic and potential energy around the x_c axis is calculated according to Fig. 1b. Kinetic energy is described by (6).

$$K_1 = \frac{1}{2}I_b\dot{\phi}^2 + 2m_w l_w^2(\dot{\phi})^2 + \frac{1}{2}I_w(\dot{\alpha_A} + \dot{\phi})^2 \tag{6}$$

Where:

- I_b : Body Inertia moment in the x_c axis (Body frame).
- I_w : Inertia moment of the Reaction wheel located on the x_c axis parallel to the rotation axis.
- $\dot{\phi}$: CubeSat angular rate in the x_c axis (Body frame).
- m_w : Mass of the Reaction wheel located on the x_c axis.
- l_w : Length from the center of the reaction wheel to the center of mass of the CubeSat.
- $\dot{\alpha_A}$: Angular rate of the Reaction wheel located on the x_c axis.

Potential energy V_1 is consider zero due to the condition of micro-gravity: $V_1 \approx 0$. Therefore, Lagrangian function is described by (7).

$$L_1 = K_1 - V_1 = \frac{1}{2}I_b\dot{\phi}^2 + 2m_w l_w^2(\dot{\phi})^2 + \frac{1}{2}I_w(\dot{\alpha_A} + \dot{\phi})^2 \tag{7}$$

Applying the Euler-Lagrange in (7) respect to angular displacement roll (ϕ) we have (8).

$$\frac{\partial}{\partial t}\left(\frac{\partial L_1}{\partial \dot{\phi}}\right) - \frac{\partial L_1}{\partial \phi} = 0$$

$$\ddot{\phi} = \frac{-I_w \ddot{\alpha_A}}{I_b + 4m_w l_w^2 + I_w} \tag{8}$$

Applying the Euler-Lagrange equation (7) respect to angular rate ($\dot{\alpha_A}$) we have (9). As can be seen in (9) we consider that the generalized forces are: 1) reaction wheel motor torque (τ_{w_A}), and 2) motor bearing friction ($B_w \dot{\alpha}_A$).

$$\frac{\partial}{\partial t}\left(\frac{\partial L_1}{\partial \dot{\alpha}_A}\right) - \frac{\partial L_1}{\partial \alpha_A} = \tau_{wA} - B_w \dot{\alpha}_A$$

$$\ddot{\alpha}_A = \left(\frac{\tau_{wA} - B_w \dot{\alpha}_A}{I_w}\right) - \ddot{\phi} \tag{9}$$

Where τ_{wA} is the x_c reaction wheel torque and B_w is the motor's coefficient of friction.

2) Equations of motion in the y_c axis (Pitch): Following the same procedure that was followed for the x-axis, the y axis movement is described by (10) and (11).

$$\ddot{\theta} = \frac{-I_w \ddot{\alpha_B}}{I_b + 4m_w l_w^2 + I_w} \tag{10}$$

$$\ddot{\alpha}_B = \left(\frac{\tau_{wB} - B_w \dot{\alpha}_B}{I_w}\right) - \ddot{\theta} \tag{11}$$

3) Equations of motion in the z_c axis (Yaw): The z axis movement is described by (12) and (13).

$$\ddot{\psi} = \frac{-I_w \ddot{\alpha_C}}{I_b + 4m_w l_w^2 + I_w} \tag{12}$$

$$\ddot{\alpha}_C = \left(\frac{\tau_{wC} - B_w \dot{\alpha}_C}{I_w}\right) - \ddot{\psi} \tag{13}$$

So, it can be seen that the CubeSat attitude for small angles its fully described by (8), (9), (11), (10), (13), and (12).

D. Reaction wheels model

To model a brushless motor, we need two equations: an electric equation and a dynamic equation [15]–[17]. Most models do not consider the effects of the slot, commutation process, and armature reaction [15]. In addition, in a three-phase motor, an approximation with a DC motor can be made due to only two phases are connected at the same time [16]. Considering that the motors we use come with their integrated driver, it is impossible to access and measure each of the phases independently. Therefore, the authors use the DC motor approximation to model the R-2418-CE motors.

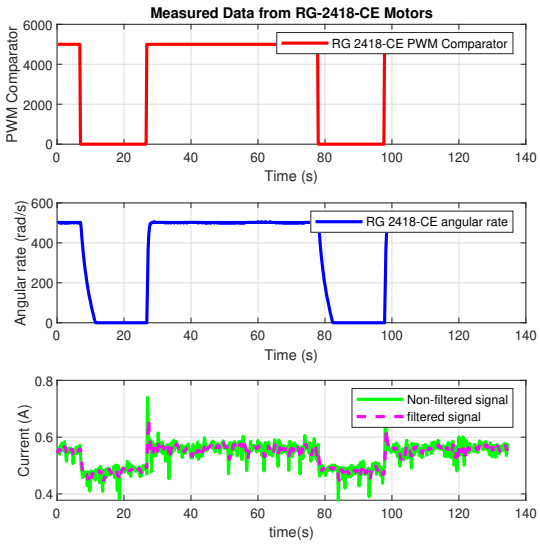

Fig. 2. R-2418-CE based Reaction Wheel response under 20 seconds pulse. The reaction wheel rate reached is 510 rad/s, the minimum reaction wheel current consumption is 470mA, and the maximum is 600mA. There is one peak of 700 mA when the pulse starts.

1) Black Box Model Identification: This article uses the Matlab ident tool to make a black box estimation for the R-2418-CE motors. Specifically, we perform a transfer function estimation with two poles and one zero in continuous time. This estimation uses the PWM timer comparator to set the duty cycle as input and the angular rate in rad/s as output.

The step response data used for estimation was with a sample time of 200ms. Also, as we mentioned earlier is not possible to measure each current phase independently; that is why the driver and all reaction wheel phases' currents were measured together.

The estimation algorithm give us the transfer function between PWM comparator and motor angular rate (Ω) as is shown in (14). The system identification had a fit estimation data of 100 percent, a Final Prediction Error (FPE) of 2.28e-27, and a Mean Square Error (MSE) equals to 2.19e-27.

$$H(s) = \frac{\Omega}{PWM} = \frac{0.225s + 0.875}{s^2 + 5.592s + 8.492} \tag{14}$$

It is essential to mention that Section IV-A describes the performed PWM settings for Tiva C and the PWM comparator characteristics.

2) Reaction Wheel Torque Calculation: Equation (4) describes relationship between Reaction wheels rates and reaction wheel torque. However, (4) is relative to orbit frame and (15) is relative to the body frame [8], [9], [18].

$$L_{rw}(t) = J_{rw}\dot{\Omega} \tag{15}$$

Due to the reaction wheel's geometry, we can use the disk inertia formula to determine J_{rw} elements. The torque transfer function can be described with (16).

$$F(s) = \frac{L_{rw}(s)}{PWM} = J_{rw}\frac{0.2252s^2 + 0.8748s}{s^2 + 5.592s + 8.492} \tag{16}$$

E. Numerical simulations

To compare both models described in II-B and II-C we perform open-loop simulations according to Table I. Fig. 3 shows the Torque applied to the CubeSat prototype, CubeSat angular rates, and Euler Angles.

TABLE I
CUBESAT OPEN LOOP PARAMETER

CubeSat Linear Parameters	
Parameter	**Values**
I_w	12.8 $\mu Kg.m$
I_b	4.26 m$Kg.m$
m_w	0.02 Kg
l_w	0.092 m
B_w	No Friction Considered.
CubeSat Non-Linear Parameters	
Parameter	**Values**
CubeSat Inertia Tensor	$\tilde{J}_B = \begin{bmatrix} 4.26 & 1.0 & 1.2 \\ 1.0 & 4.26 & 1.2 \\ 1.2 & 1.2 & 4.26 \end{bmatrix} \times 10^{-3}$ (Nm)
Reaction wheels parameters	
Parameter	**Values**
Radius	$R_{rw} = 4.3$ cm
Mass	$m_{rw} = 20$ g
Width	$d_{rw} = 1.5$ cm

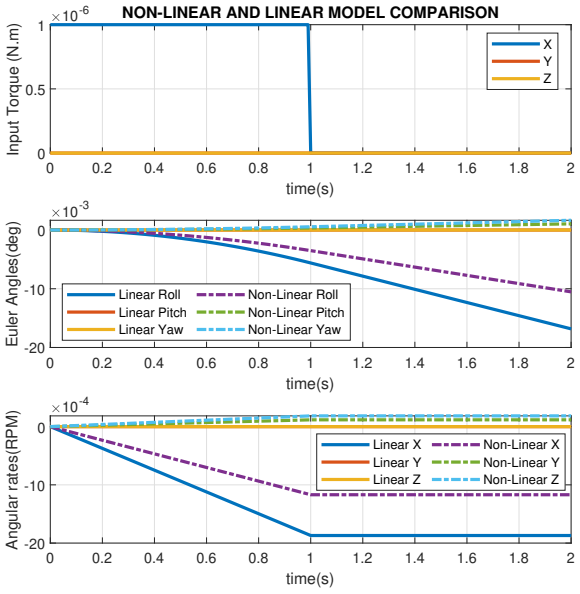

Fig. 3. CubeSat dynamics under a torque pulse input of 1e-6N.m for one second on the reaction wheel over the X_c Axis. The dotted line represents non-linear system outputs and the solid lines are outputs of the linear system.

As shown in Fig. 3, the non-linear and linear systems have a similar behavior until the Roll Euler Angle keeps < 1 second, where the difference between both systems is 0.38 degrees. On the other hand, the X_c angular body rates in the non-linear model reach -1.1e-1 RPM, and in the linear model, it reaches -1.8e-1 RPM. As can be seen, the linear model does not consider the effect of one axis rate on the other axis; However, these velocities are low (in the order of 1.5e-4 RPM) in the Y_c and Z_c axis.

F. Friction Model

In Fig. 3 the simulations does not consider any disturbance force and friction. However, in the implementation a friction influence in the angular rates was measured. Fig. 4 shows the measured angular rates under a step input of -3.96E-03 Nm in Z_c axis without any control. As can be seen, the influence of viscous friction caused by the air bearing tends to stop the angular rate grow in the Z_c axis to 8.09 rad/s. Fig. 4 also shows simulation of friction model. The considered friction model is a modification of (3) to obtain (17).

$$\dot{\omega} = J_B^{-1}\left[L - L_{rw} - \omega \times (J_B\omega + J_{rw}\left[\omega + \Omega\right])\right] - a\omega \quad (17)$$

Where a is in the R^{1x3} field and represents the viscous coefficient friction. After a identification process we found $a = 2.95E-2[1,1,1]$.

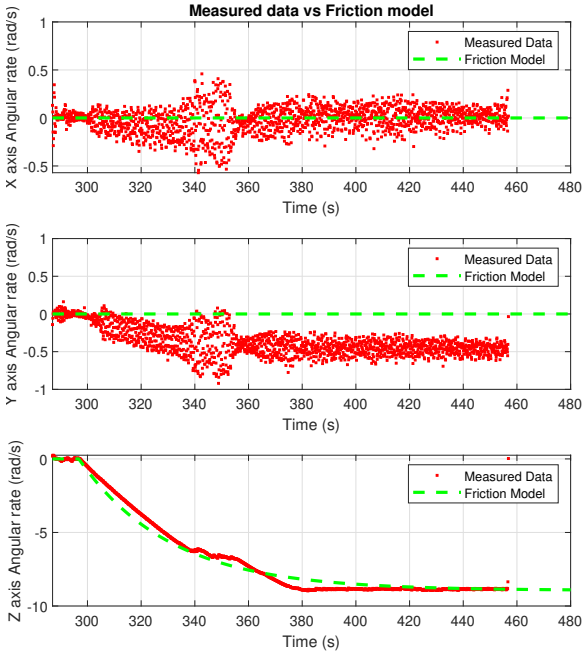

Fig. 4. Comparison between measured data and the proposed model considering an friction coefficient of 2.95E-2. Under a step input of -3.96E-03 Nm in Z axis and with an air bearing pressure of 30 PSI.

III. DESIGN AND IMPLEMENTATION

A. Testing platform

As shown in Fig. 5 the system's testing platform has two parts: 1, Static Plate and 2, Dyson Sphere. Fig. 6a shows the Static Plate and the Dyson sphere.

1) **Static Plate or Stator:** The static plate maintains constant pressure towards the center of the Dyson sphere by placing six holes symmetrically with a diameter of 0.7 mm. Through them, air flows at pressures of approximately 30 to 40 psi.

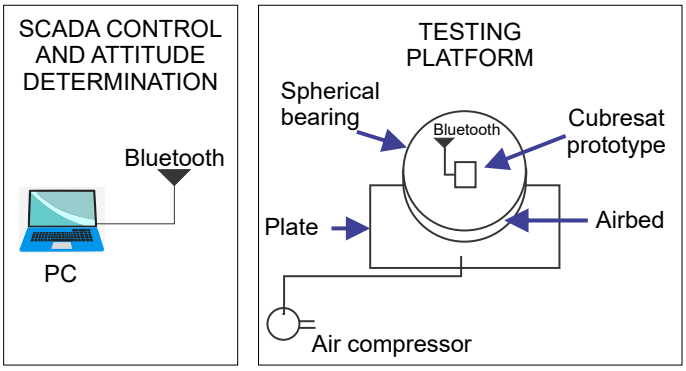

Fig. 5. The proposed design is composed of a SCADA control and a testing platform. The testing platform is composed of a Dyson sphere and a static plate. Both produce a spherical air bearing between them. Besides, the Dyson sphere does not alter the CubeSat's gravity center.

2) **Dyson Sphere or Rotor:** It is a sphere that surrounds the CubeSat and distributes the plate's air over its surface to reduce friction.

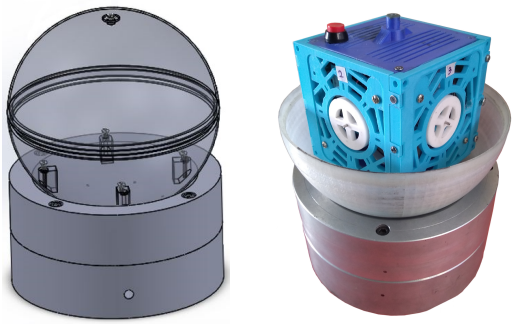

(a) Static Plate and Dyson sphere (b) CubeSat structure

Fig. 6. (a) Static Plate and Dyson sphere form a spherical air bearing to reduce friction and simulate non-gravity conditions. (b) The proposed CubeSat structure has three Reaction Wheels on each axis and supports attached to a Dyson sphere.

B. CubeSat prototype

1) **Implemented Reaction wheels:** R-2418-CE motors and disks of 2.5 grams with a diameter of 2cm implement the Reaction wheels. Our designed reaction wheel's maximum inertia moment can reach is about 5.00e-7 $kg.m^2$. Table II shows the R-2418-CE technical characteristics.

2) **CubeSat structure:** The CubeSat structure is made by 3D printing with the standard dimensions of 1U CubeSat (10cm x 10cm) as Fig. 6b depicts. Table III shows the CubeSat's weights and parameters with the associated electronics.

C. On board computer and electronics

CubeSat's electronics have three subsystems: 1) the Reaction wheels driver, 2) The power supply subsystem, and 3) the control subsystem. Fig. 7 shows a block diagram of the overall system.

TABLE II
R-2418-CE BRUSHLESS MICROMOTORS TECHNICAL SPECIFICATIONS

Technical specifications	
Speed	4500 RPM
Vcc	12 VDC
PWM	0.5 - 60 khZ
Encoder resolution	18 pulses per revolution.
Pins	Red: Vcc
	Black: GND
	Yellow: FG (Hall encoder)
	White: PWM
	Orange: CCW/CW

TABLE III
CUBESAT'S STRUCTURE WEIGHTS AND DISTRIBUTION IN EACH AXIS.

CubeSat Prototype Distribution		
CubeSat's face	**Axis**	**Weight (g)**
Upper face	Z	25
Structure and Reaction Wheel	X	65
Structure and Reaction Wheel	Y	62
Structure and Control Circuit	-X	59
Structure and Power Circuit	-Y	68
Structure and Reaction Wheel	-Z	59
Battery	Z	69

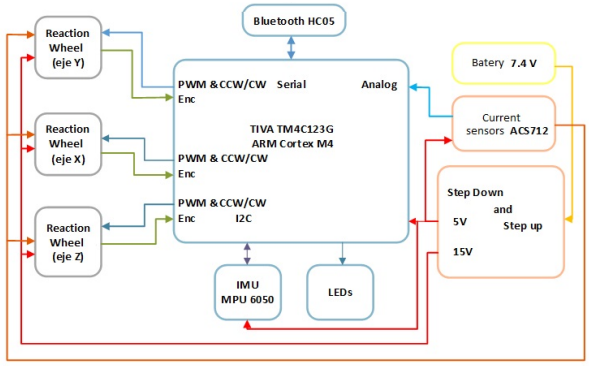

Fig. 7. Electronics block diagram implemented in the CubeSat prototype for data acquisition and transmission to the monitoring software.

1) **Reaction wheels driver:** The MS88291 circuit embedded into the R-2418-CE motors implements the reaction wheel's drivers. Its control pins are shown in Table II and have an operating range between 3.3 and 5volts. However, despite its wide range of operations, the encoder signal always operates with 5 volts.
2) **Power supply subsystem:** The power supply subsystem is composed of LM2596, XL6009 circuits, and a 1000mA-7.4DCV lipo battery. This subsystem is used to power the overall system with 5DCV and 15DCV.
3) **Control and monitoring subsystem:** The control subsystem carries out attitude control, transmission, and data acquisition. It comprises an IMU MPU6050, three ACS712 current sensors, and a Bluetooth HC05 module. The ARM Cortex TM4C123G microcontroller was cho-

sen as an onboard computer due to its high computing performance.

D. Software interface for monitoring

The monitoring interface was developed in LabVIEW. This software allows monitoring the CubeSat sensors: 1) Reaction wheels current sensors, 2) Encoder sensors, and 3) IMU MPU6050. The proposed interface is shown in Fig. 8.

IV. Monitoring and control algorithms

The CubeSat prototype has a multi-thread algorithm to perform control, transmission, and data acquisition. This chapter is divided into three subsections to explain the initial settings, the monitoring algorithms, and the control algorithm.

A. Initial Settings

The initial settings are performed in the main thread, as Fig. 9 depicts. Here, we configure all the hardware interruptions, initialize PWM modules, set the MPU6050 sensor, and configure timers as a Counter in Input-Edge Count Mode to read reaction wheel encoders.

1) PWM Modules Settings: We used the module PWM1 with generators 2A, 3A, and 3B to manage the reaction wheel rates with PWM signals. This paper uses the M1pwm5, M1pwm6, and M1pwm7 outputs. Besides, the PWM configuration is performed with the following guidelines.

1. Enable clock for PWM1 module and associated GPIO's.
2. Enable System Clock Divisor with a pre-scaler value of 64.
3. Setting GPIOs as PWM channels.
4. Enable PWM Generator and select down count mode.
6. Configure PWM channel to set PWM output when counter reloaded and clear when matches PWMcmp value.
7. Set PWM frecuency for 50Hz with a PWMload value of 5000.
8. Set duty cycle through PWMcmp value.

With the guidelines mentioned above, we can control the duty cycle by variating the PWMcmp register between 0 and 4999 to obtain a duty cycle of 100% to 0%, respectively.

2) Timers as Counters in Input-Edge: To get reaction wheel rates, we configure timers 0A, 0B, and 2A in Up-count, edge-count, and capture mode. These configurations allow us to count each rising edge coming from the encoder signal, and they run parallel to the main thread.

B. Monitoring algorithms

Monitoring algorithms consist of two different threads, as seen in Fig. 9. The first thread manages the Analog-Digital-Converter 0 (ADC0) and generates interruptions through the ADC Sequencer 2 (ASS2) triggered by a timer each 200ms. The associated interrupt manages the ACS712 current sensors and performs a mobile-average filter with a window size of 20 samples.

The second thread manages the UART communication. An HC-06 module is connected through the UART5 port to send data to a PC and vice-versa. The associated interrupt is triggered each time the Rx buffer is half full.

We can consider as other threads the timers configured as a Counter in Input-Edge capture mode to measure reaction Wheels rates due to the hardware counters running parallel.

C. Control algorithms

We perform the control algorithms in a third thread to ensure a proper sample time. The SysTick timer interrupt is used to perform the reaction Wheels Torque controllers and a PID Attitude control, as can be seen in Fig. 10.

In Fig. 10 we talk about the "perform torque controller" and "calculate the current torque" functions. The first function is proposed as Fig. 11. It is easy to see that the torque controller is based on the transfer function (16), so it is necessary to calculate the current torque with the function "Calculate current torque," which is based on equation (15).

In addition, the systick thread has a function called "Perform attitude Control Law" as his name says this function perform the attitude control algorithm. In this paper we develop a basic PID attitude controller to perform small attitude maneuvers. The way that we connect attitude control and torque control can be seen in Fig. 12. Finally, Fig. 13 depicts the bode plot of the designed control system roll axis. The positive phase and gain margin shows a stable system. Similarly, due to the CubeSat prototype is symmetric and independent for small angles, we can ensure that pitch and yaw angles control loops have the same characteristics.

V. Conclusions and Discussion

This article develops the design, simulation, and preliminary construction of a based air-bearing test system for attitude control with low-cost materials. Its principal aim is to provide the Universidad Nacional de San Agustin de Arequipa (UNSA) with a modulus to teach attitude control and encourage students to follow the aerospace engineering field. Up to this stage, the proposed modulus is only operative for educational purposes because an actual satellite is composed of several subsystems. The proposed attitude determination control algorithm and sensors in this modulus differ from real satellites. According to the requirements, several sensors such as sun sensors, horizon sensors, star trackers, gyros, and magnetometers can be used in conjunction with a sensor fusion Kalman algorithm to reach Euler Angles errors in the order of 0.001 degrees. In our design, only the MPU6050 data is used to obtain CubeSat's Euler Angles, and errors sources like the Allan Randon walk and gyroscope offset affect the final results producing drift errors that must be removed. In future versions an attitude and heading reference system (AHRS) algorithm will be implemented with a magnetometer in order to reduce attitude drift errors.

Each reaction wheel rate and current is acquired and processed in the proposed monitoring algorithm with mobile average filters. The ADC measurement is performed each 200ms because its use is only for monitoring, and its low

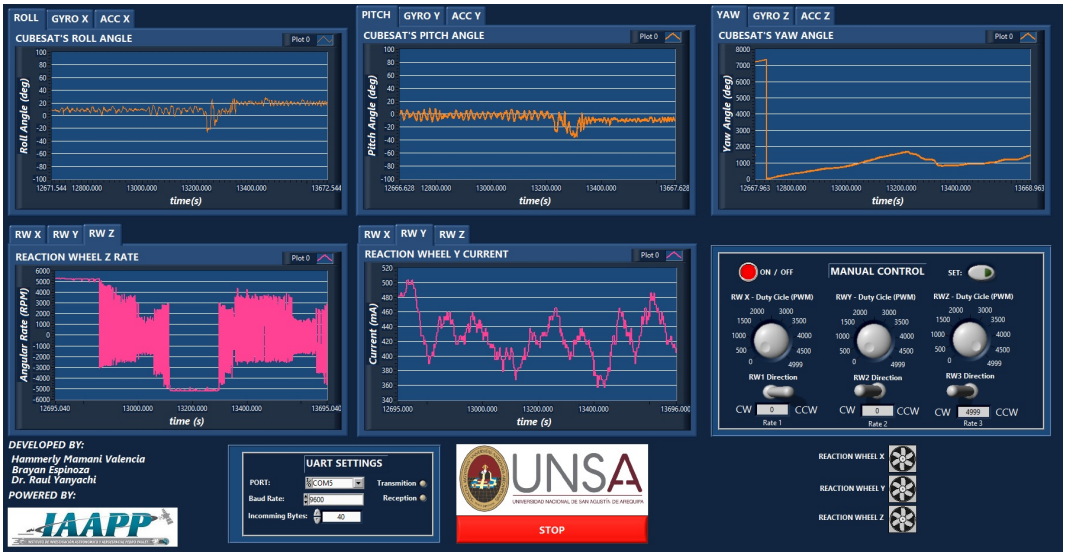

Fig. 8. The proposed interface program was developed in Labview 2020. This interface can handle UART settings and data acquisition in real-time. In the manual control mode, the three potentiometers can handle reaction wheel rates and direction.

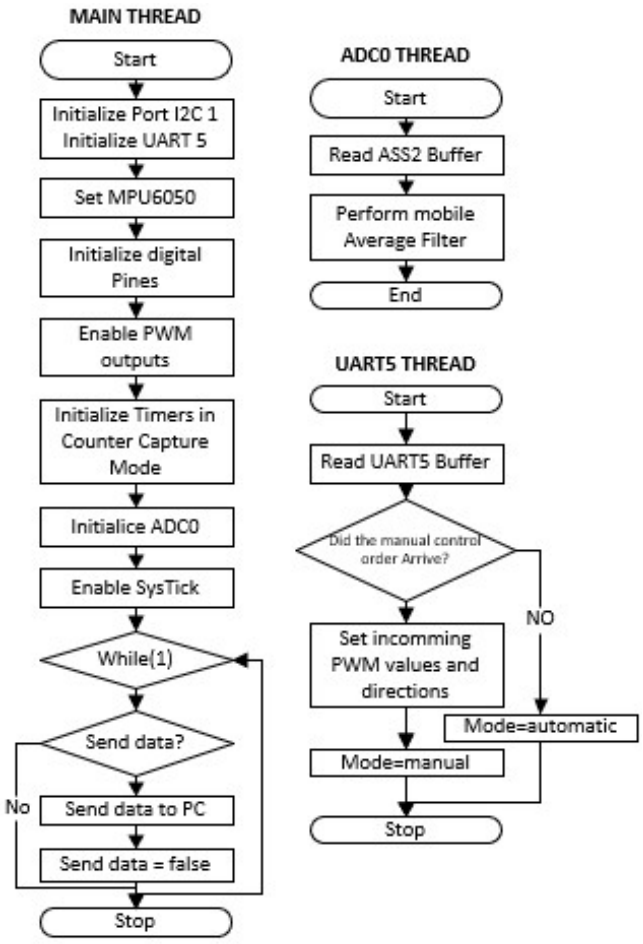

Fig. 9. Main thread, ADC0 thread, and UART5 Thread configured as hardware interrupts to perform parallel tasks. Timers in capture count mode is not shown in this image because they don't affect flow chart.

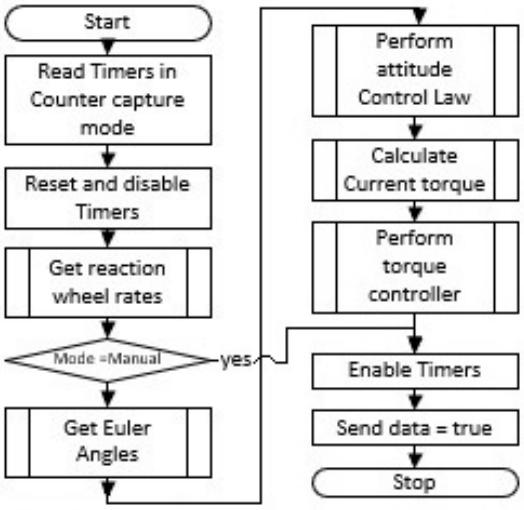

Fig. 10. Systick thread to get Euler angels, Calculate current torque and perform control algorithms. This thread runs parallel to the other threads but with the highest priority.

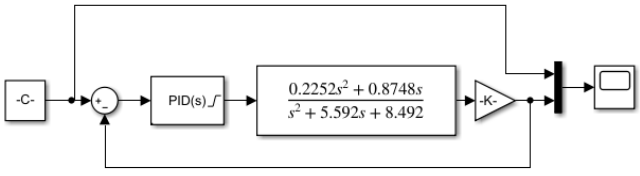

Fig. 11. Proposed reaction wheel torque controller based in the black box model estimation. This PID controller only has a integral part with a Ki coefficient of 1.567e10.

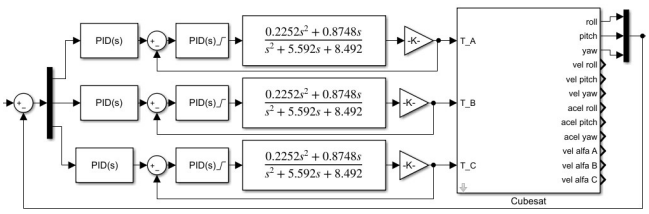

Fig. 12. Proposed controller algorithm for a CubeSat. A linear PID controller is used to control attitude in each axis. The PID coefficients are adjusted as: Kp=-3.249e-07, ki=-2.196e-10, kd=-8.465e-05.

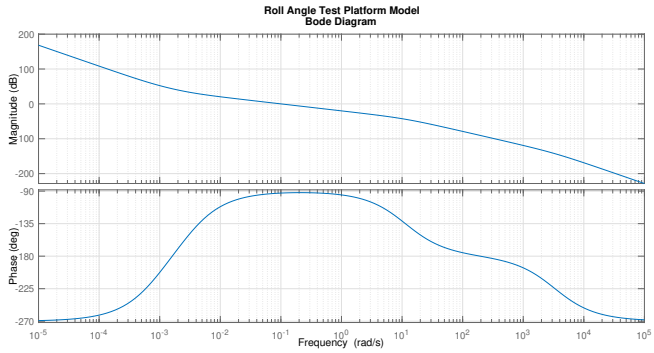

Fig. 13. Bode plots of the Roll angle control loop. The margin phase is 87.32 deg and the gain phase is 41.05. Phase and gain margins shows a stable system.

sample time helps us better manage the microcontroller resources. Reaction wheel rates are measured through timers in counter edge capture mode, which can run parallel. However, to give us correct data, it is necessary to count rising edges for almost 100ms. A way to improve these measurements is with the timers in time input edge-captured mode, which starts a timer when a rising edge is detected and stops when the edge is detected again. This configuration will be helpful to read the encoder's signal frequency and obtain the RPM speed indirectly. The problem with the second way to measure reaction wheel rates is that this process needs to use interrupts which can be triggered with a frequency of 1.5Khz (maximum encoder frequency), and the timer continues running until the interrupt is performed. This configuration works well when this is the only thread we use. A way to improve that problem is to use another microcontroller to handle reaction wheel rate measurements and communicate with the Tiva C.

Likewise, the direction and speed of each reaction wheel are controlled through PWM signals and digital pines. It is essential to notice that the modeled CubeSat's controller is only valid for small angles. Due to our own designed reaction wheels, we can perform two degrees attitude maneuver as maximum. We need to increase the maximum torque to achieve large-angle maneuvers and not reach saturation. We also notice that our proposed design must choose a significant settling time due to the dead time in torque controllers. In another way, the torque controller will not be able to track the command torque. Finally, the proposed mathematical model does not have into considerations perturbations generated by air bearing viscous drag. According to [4] the test bed perturbations are proportional to the air flow in the spherical air bearing that's why the maximum CubeSat prototype weight is 1kg in other case the perturbations produced by air flow will become the system unstable. In future versions of the modulus we will increase the Reaction wheels' torque and we will quantify the torque produced by air flow.

ACKNOWLEDGMENT

The authors are grateful for the support provided by the Center for Acquisition and Processing of Satellite Data (CAPDS) located in the Pedro Paulet Astronomical and Aerospace Institute (IAAPP) of the Universidad Nacional de San Agustin de Arequipa.

REFERENCES

[1] C. Nieto-Peroy and M. R. Emami, "Cubesat mission: From design to operation," *Applied Sciences*, vol. 9, no. 15, 2019.
[2] N. Jovanovic, J. M. Pearce, and J. Praks, "Design and testing of a low-cost, open source, 3-d printed air-bearing-based attitude simulator for cubesat satellites," *Journal of Small Satellites*, vol. 8, no. 2, pp. 859–880, 2019.
[3] H. Woo, O. Rico, S. Chesi, and M. Romano, *CubeSat Three Axis Simulator(CubeTAS)*, ch. 1. AIAA, 2011.
[4] T. Rybus and K. Seweryn, "Planar air-bearing microgravity simulators: review of applications, existing solutions and design parameters," *Acta Astronautica*, vol. 120, pp. 239–259, 2016.
[5] J. L. Schwartz, M. A. Peck, and C. D. Hall, "Historical review of air-bearing spacecraft simulators," *Journal of Guidance, Control, and Dynamics*, vol. 26, no. 4, pp. 513–522, 2003.
[6] L. Schwartz Jana, A. Peck Mason, and D. Hall Christopher, "Historical review of spacecraft simulators," *Advances in the Astronautical Sciences*, vol. 114, pp. 405–423, 2003.
[7] A. Mehrparvar, D. Pignatelli, and J. Carnahan, "Cubesat design specification," *The CubeSat Program*, 2014.
[8] H. Marquez, "Nonlinear control systems: Analysis and design," *Wiley & Sons*, 11 2002.
[9] B. A. Espinoza Garcia, "Non-linear control strategies for attitude maneuvers in a cubesat with three reaction wheel," *Universidad Nacional de San Agustín de Arequipa*, 2021.
[10] P. R. Yanyachi Aco Cárdenas, "Modelagem e controle de atitude de satélites artificiais com apêndices flexíveis," 2005.
[11] M. Gajamohan, M. Merz, I. Thommen, and R. D'Andrea, "The cubli: A cube that can jump up and balance," in *2012 IEEE/RSJ International Conference on Intelligent Robots and Systems*, pp. 3722–3727, IEEE, 2012.
[12] M. Muehlebach and R. D'Andrea, "Nonlinear analysis and control of a reaction-wheel-based 3-d inverted pendulum," *IEEE Transactions on Control Systems Technology*, vol. 25, no. 1, pp. 235–246, 2016.
[13] J. Aparicio Jiménez, "Attitude control board for cubesat," 6 2019.
[14] M. J. Sidi, *Spacecraft dynamics and control: a practical engineering approach*, vol. 7. Cambridge university press, 1997.
[15] C. Huang, F. Lei, X. Han, and Z. Zhang, "Determination of modeling parameters for a brushless dc motor that satisfies the power performance of an electric vehicle," *Measurement and Control*, vol. 52, no. 7-8, pp. 765–774, 2019.
[16] J. A. Becerra-Vargas, F. E. Moreno-García, J. J. Quiroz-Omaña, and D. Bautista-Arias, "Estimación de parámetros y modelo de caja negra de un motor cd sin escobillas," *TecnoLógicas*, 2014.
[17] H. S. Hameed, "Brushless dc motor controller design using matlab applications," in *2018 1st International Scientific Conference of Engineering Sciences-3rd Scientific Conference of Engineering Science (ISCES)*, pp. 44–49, IEEE, 2018.
[18] Y. Yang, "Spacecraft attitude and reaction wheel desaturation combined control method," *IEEE Transactions on Aerospace and Electronic Systems*, vol. 53, no. 1, pp. 286–295, 2017.